

PAPER

A new coupling mechanism between two graphene electron waveguides for ultrafast switching

To cite this article: Wei Huang *et al* 2018 *Semicond. Sci. Technol.* **33** 035014

View the [article online](#) for updates and enhancements.

Related content

- [Transmission in graphene through time periodic double barrier potential](#)
Miloud Mekkaoui, El Bouâzzaoui Choubabi, Ahmed Jellal et al.
- [Mesoscopic devices](#)
T J Thornton
- [All-graphene field-effect transistor based on lateral tunnelling](#)
D Svintsov, V Vyurkov, A Orlikovsky et al.

A new coupling mechanism between two graphene electron waveguides for ultrafast switching

Wei Huang¹, Shi-Jun Liang¹ , Elica Kyoseva² and Lay Kee Ang¹

¹SUTD-MIT International Design Centre, Singapore University of Technology and Design, 8 Somapah Road, 487372, Singapore

²Institute of Solid State Physics, Bulgarian Academy of Sciences, 72 Tsarigradsko Chaussée, 1784 Sofia, Bulgaria

E-mail: shijun_liang@mymail.sutd.edu.sg, elkyoseva@gmail.com and ricky_ang@sutd.edu.sg

Received 15 September 2017, revised 9 December 2017

Accepted for publication 5 January 2018

Published 15 February 2018



CrossMark

Abstract

In this paper, we report a novel coupling between two graphene electron waveguides, in analogy the optical waveguides. The design is based on the coherent quantum mechanical tunneling of Rabi oscillation between the two graphene electron waveguides. Based on this coupling mechanism, we propose that it can be used as an ultrafast electronic switching device. Based on a modified coupled mode theory, we construct a theoretical model to analyze the device characteristics, and predict that the switching speed is faster than 1 ps and the on–off ratio exceeds 10^6 . Due to the long mean free path of electrons in graphene at room temperature, the proposed design avoids the limitation of low temperature operation required in the traditional design by using semiconductor quantum-well structure. The layout of our design is similar to that of a standard complementary metal-oxide-semiconductor transistor that should be readily fabricated with current state-of-art nanotechnology.

Keywords: graphene, electron waveguide, electronic switching, transistor-like

(Some figures may appear in colour only in the online journal)

1. Introduction

Graphene's extremely-high mobility enables the promising application in electronics, but it is notoriously difficult to have a high turn on and off ratio due to the lack of a band gap for single-layer field-effect transistors (FET) [1, 2]. There have been some extensive research activities in the exploration of novel approaches to achieving high on–off ratios graphene FET, such as utilization of uniaxial strain [3], lateral confinement [4] and breaking inversion symmetry [5], in order to create a band gap in single-layer graphene. Another approach is to exploit transport band gap based on few-layer graphene under perpendicular electric field [6]. A recent approach utilizes the unique electron transport in graphene, called electron optics mechanism in p–n junctions [7, 8]. Unfortunately, the on–off ratio of graphene FET based on above proposals is still lower than 10^6 even at higher large bias [9, 10].

In this paper, we will explore the coupling between two graphene electronic waveguides based on the coherent quantum mechanical tunneling of Rabi oscillation. The concept of electron waveguide was first proposed in the 90s in analogy to the optical waveguide [11–17], where the electrons are trapped in a quantum well structure composed of AlGaAs/GaAs material and ballistic electron transport is assumed. Based on this electron waveguide with AlGaAs/GaAs quantum well structure, the researchers described the coupling mechanism between two electron waveguides based on coupled mode theory (CMT) and proposed the concept of electron switching device based on electron waveguide. These types of electron waveguide switches are expected to have ultrafast operating speed. Recent calculations show that the operating frequency of such a device is up to $0.5 \times 10^{12} \text{ s}^{-1}$ and the maximum coupling energy between the waveguides is 10 meV [12, 13], which corresponds to a very short coupling length of about 280 nm. Despite these

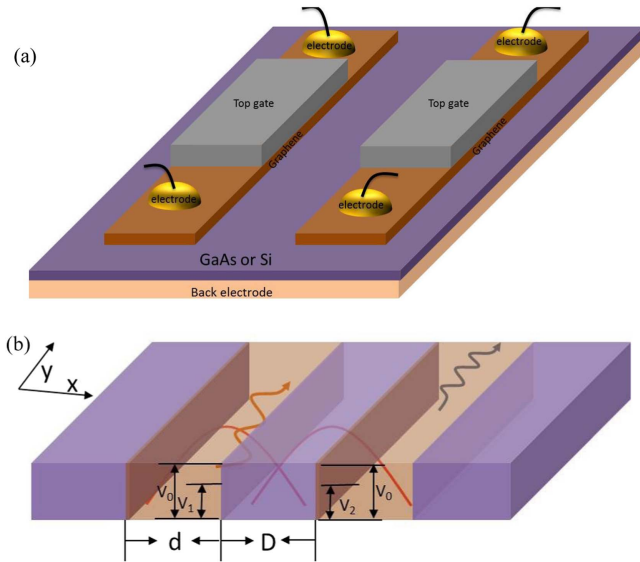


Figure 1. (a) The scheme of ultra-fast electron switch based on dual graphene electron waveguide. (b) The corresponding energy band structure of (a). V_0 is the Schottky barrier height between graphene and GaAs or silicon material and V_1 , V_2 are the bias voltages applied to modulate the coupling length between the two graphene waveguides. d is the width of the graphene quantum wells and D is the distance between the two graphene electron waveguides.

encouraging predictions, it has never been realized experimentally at room temperature probably due to the unjustified assumption of long electron mean free path at the interface of AlGaAs/GaAs material at room temperature that the electrons will suffer inelastic scattering and the coherent phase of the wave packet can not be maintained. Thus, an electron waveguide based on AlGaAs/GaAs materials at room temperature may not be practical for ultrafast switching application as ultra-low temperature (typically below 4 K) is required [14].

This limitation may be lifted with the advances in using graphene electron waveguide [18–22], which has successfully demonstrated ballistic electron transport in a quantum well created on graphene on the length scale of a few μm . Tunable Fermi level in the graphene via gating voltage will also offer additional control over the performance of electronic switching device as the tunable barrier height formed at the interface of graphene and different semiconductors (e.g. Si and GaAs) have been confirmed both experimentally and theoretically [23–26], and thus provides another advantage over the fixed band offset at the interface of AlGaAs/GaAs material. All these new findings may enable a high on–off ratio electronic switching device by using graphene-based electron waveguide.

In this paper, firstly, we introduce CMT to determine the coupling between two parallel graphene electron waveguides, which may serve as a novel ultrafast electronic switching device, in analogy to the optical dual-channel waveguide device. The schematic diagram of the proposed design is shown in figure 1. As compared to the AlGaAs/GaAs quantum well structure, there are three main advantages as summarized below. Firstly, graphene electron waveguide has long electron

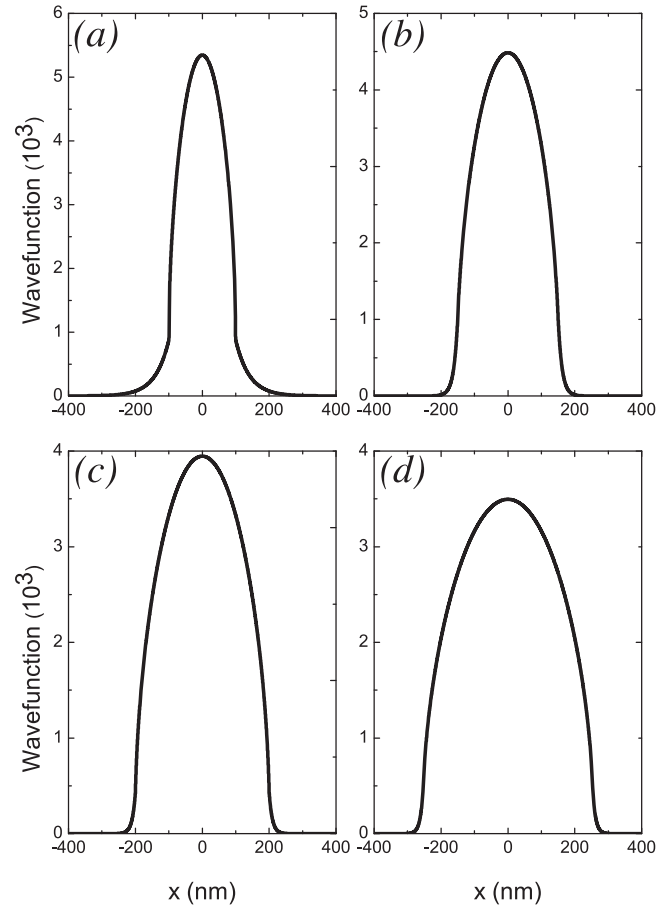


Figure 2. The symmetrical wave modes of first mode $u_1 = u_2 = \psi_A - i\psi_B$ in the graphene electron waveguide for different widths d of the quantum well. Schottky barrier height between graphene and AlGaAs/GaAs is 500 meV and $V_1 = V_2 = 450$ meV, so that the effective barrier height between the two graphene waveguides is 50 meV and $k_1 d = 4.96\pi$. (a) $d = 200$ nm, $k_{1x} d = 2.9465$, $\theta = 79.1^\circ$, (b) $d = 300$ nm, $k_{1x} d = 3.0243$, $\theta = 78.809^\circ$, (c) $d = 400$ nm, $k_{1x} d = 3.1165$, $\theta = 78.463^\circ$, (d) $d = 500$ nm, $k_{1x} d = 3.0554$, $\theta = 78.669^\circ$.

mean free path, about 4–10 μm [27] at room temperature, which may be larger than the characteristic length of the device. Secondly, graphene material has tunable Fermi energy level via gating voltage. Lastly graphene electron waveguide can operate at room temperature. According to our calculated results (see figures 2 and 3), we predict that the switching time is faster than 1 ps (as shown in figure 4) and a very high on–off ratio (exceeds 10^6 , as shown in figure 5).

2. CMT of graphene electron waveguide

CMT was initially developed for guided-wave optics to describe the coupling between adjacent optical waveguides, due to the overlap of their evanescent electromagnetic fields. This allows light to be transferred robustly between the optical waveguides [28–30]. By drawing the analogy between the wave nature of electrons (as massless particles) traveling inside the graphene to electromagnetic waves in optical waveguides, CMT is revised to describe the coupling between

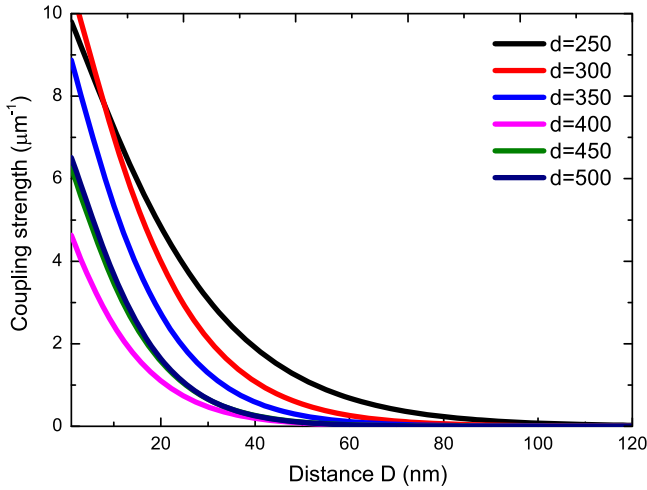


Figure 3. The coupling strength between two parallel graphene electron waveguides with fixed $k_1 d = 4.96\pi$ as a function of spacing D between graphene electron waveguides at the different width of the waveguide d .

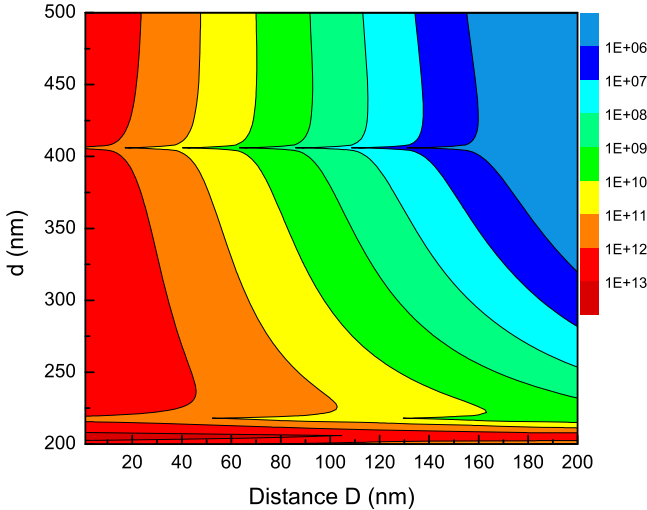


Figure 4. Contour plot of complete transfer frequency as a function of the width d of quantum well and distance D between two graphene electron waveguides. We set $k_1 d = 4.96\pi$ and Schottky barrier height between graphene and GaAs is 500 meV. $V_1 = V_2 = 450$ meV.

two parallel graphene electron waveguides as shown in figure 1. When the graphene electron waveguides are closely positioned, electrons can be efficiently coupled. For the proposed electron switching device, we assume that the two bias gate voltages V_1 and V_2 are equal, thus realizing an electron tunneling version of the Rabi oscillations. Based on CMT, the coupling length L will depend on a coupling parameter defined as $\Omega = C_{1/2}$ (see definition below) between the two graphene waveguides, namely $L = (2n + 1)\pi/\Omega$, where n is integer, $f_T = v_f/L$ is the transition frequency, and $v_f = 10^6$ m s⁻¹ is the Fermi velocity of electrons in graphene.

In our two-dimensional model (see figure 1), the proposed ultrafast quantum FET behaves like an electron

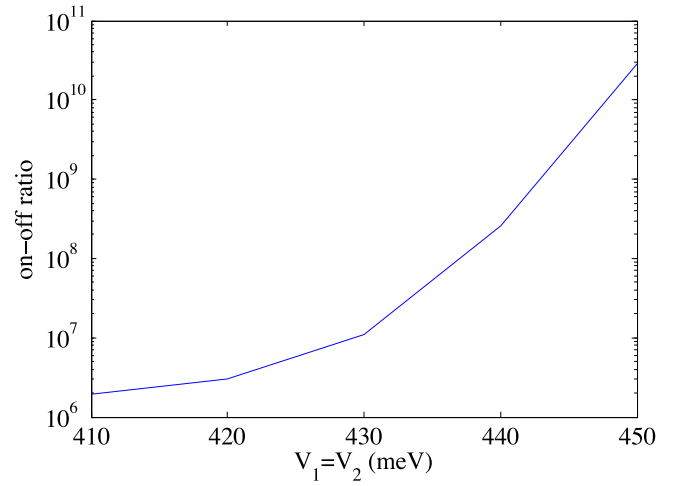


Figure 5. On-off ratio with varying $V_1 = V_2$ from 410 to 450 meV. We set $d = 200$ nm and the energy of injection electron is $E = 498.28$ meV. Schottky barrier height between graphene and GaAs to be 500 meV. The device length set to be 654 nm, which is the coupling length L for $V_1 = V_2 = 450$ meV.

switching device consisting of two parallel graphene electron waveguides. The width of the waveguide is d and the separation of the two waveguides is D . Aligned with the standard complementary metal-oxide-semiconductor (CMOS) FET terminology, the two parallel graphene waveguides can be regarded as a source waveguide and a drain waveguide. For each graphene waveguide, the two ends are referred as its input and output for the electrical signal. The ohmic contact between the metal electrodes and the graphene is assumed to enable sufficient electron injection into the waveguides.

When a small voltage is applied to the left graphene waveguide, an electrical current can be measured at the outputs of both graphene waveguides. The gate voltages (V_1 and V_2) on each graphene waveguide are used to tune the Fermi level of each channel independently. Consequently, the Schottky barrier height (V_0) and thickness layer (D) between the graphenes can be modulated. If the Schottky barrier height and the effective gap spacing between the two graphene waveguides are sufficiently small, the evanescent wave of the injected electrons in the source waveguide can tunnel into the drain waveguide with some probability as represented by the red curve in figure 1(b), which can be defined as an on-state. When the Schottky barrier height and effective gap spacing become large due to the applied gate voltage, the tunneling probability of electron tunneling from source waveguide to drain waveguide is extremely small, which can be defined as an off-state. (In our example, we set off-state of gate voltages as $V_1 = V_2 = 300$ meV.) Note that the phase of the electrons is maintained during the tunneling process. Quantum mechanically, the injected electrons in the source waveguide can be detected at the drain waveguide with a probability equal to 1 (see black curved arrow in figure 1(b)) at a certain transfer length L .

In our model, we assume that a quantum well is created at the interface between the graphene and GaAs. The electrons in

the graphene waveguides are confined along with the x -direction, and they unbounded in the y -direction. The total electron wave function is the superposition of all possible quantum eigenstates. We make the notations $\Psi_1(x, y)$ ($\Psi_2(x, y)$) as the electron wave function of source (drain) graphene waveguide, which is written as

$$\begin{aligned}\Psi_1(x, y) &= \sum_m a_{1m}(y) u_{1m}(x) \exp(-i\beta_{1m}y), \\ \Psi_2(x, y) &= \sum_n a_{2n}(y) u_{2n}(x) \exp(-i\beta_{2n}y),\end{aligned}\quad (1)$$

where a_{1m} , a_{2n} are m th, n th modes with respect to source/drain graphene waveguide. Here, $u_{1m}(x)$, $u_{2n}(x)$ are the mode profiles of the wavefunctions determined by electron eigenstates in the quantum well, where m , n are the mode indexes. $\beta_{1m} = k_1 \sin(\theta_m)$ and $\beta_{2n} = k_2 \sin(\theta_n)$ are the respective propagation constants of the m th and n th modes in graphene electron waveguide with respect to source/drain graphene waveguide. The parameters θ_m and θ_n describe the injection electron angles with respect to the corresponding m th and n th modes in the source/drain graphene waveguide, k_1 and k_2 are the wave vectors of electron injected in the source/drain graphene waveguide: $k_1 = (E - V_1)/\hbar v_F$ and $k_2 = (E - V_2)/\hbar v_F$. The wave vector in the barrier material is $k_0 = \sqrt{-2m_{\text{eff}}(E - V_0)/\hbar^2}$, where E is the electron energy and m_{eff} is the electron effective mass in the semiconductor material.

According to Myoung's paper [31], the electron's wave function behaves as a plane wave along with the y direction and equation (1) can be rewritten as

$$\begin{aligned}\Psi_1(x, y) &= \sum_m a_{1m}(y) \psi_{1m}, \\ \Psi_2(x, y) &= \sum_n a_{2n}(y) \psi_{2n},\end{aligned}\quad (2)$$

where $\psi_{1m} = u_{1m}(x) \times \exp(-i\beta_{1m}y)$ and $\psi_{2n} = u_{2n}(x) \times \exp(-i\beta_{2n}y)$. In the y direction, the motion of the electrons in the graphene electron waveguides is described by the 1D free electron Dirac equation, which allows us to decouple the wavefunctions into two sublattices: A and B wave functions (see the appendix for details). Finally, two Helmholtz-like equations in the y direction are obtained as

$$\begin{aligned}\frac{\partial^2}{\partial y^2} \psi_{1m} + \beta_{1m}^2 \psi_{1m} &= 0, \\ \frac{\partial^2}{\partial y^2} \psi_{2n} + \beta_{2n}^2 \psi_{2n} &= 0.\end{aligned}\quad (3)$$

Based on the CMT model [28] we can manipulate the Helmholtz equations to obtain

$$\begin{aligned}\frac{\partial^2}{\partial y^2} \Psi_{1m}(x, y) + \beta_{1m}^2 \Psi_{1m}(x, y) &= -(k_2^2 - k_0^2) \Psi_{2n}(x, y), \\ \frac{\partial^2}{\partial y^2} \Psi_{2n}(x, y) + \beta_{2n}^2 \Psi_{2n}(x, y) &= -(k_1^2 - k_0^2) \Psi_{1m}(x, y),\end{aligned}\quad (4)$$

which are consistent with previous optical waveguide coupled equations [32] and the electron waveguide coupled equations [11].

By substituting equation (1) into (4), and considering ψ_{1m} and ψ_{2n} obeying equation (3), we apply the slowly envelope varying approximation (SEVA) [32] to equation (4), such that $\frac{d^2 a_1}{dy^2} \ll \frac{da_1}{dy}$ and $\frac{d^2 a_2}{dy^2} \ll \frac{da_2}{dy}$, and obtain the following coupling equations:

$$\begin{aligned}\frac{da_{1m}}{dy} e^{-i\beta_{1m}y} &= -iC_{12} a_{2n} e^{-i\beta_{2n}y}, \\ \frac{da_{2n}}{dy} e^{-i\beta_{2n}y} &= -iC_{21} a_{1m} e^{-i\beta_{1m}y}.\end{aligned}\quad (5)$$

Here, C_{12} and C_{21} are the coupling coefficients, which are given by,

$$\begin{aligned}C_{12} &= \frac{1}{2} \frac{k_2^2 - k_0^2}{\beta_{1m}} \int_{-\infty}^{+\infty} u_{1m}(x) u_{2n}(x) dx, \\ C_{21} &= \frac{1}{2} \frac{k_1^2 - k_0^2}{\beta_{2n}} \int_{-\infty}^{+\infty} u_{1m}(x) u_{2n}(x) dx.\end{aligned}\quad (6)$$

Finally, equation (5) can be rewritten as a Schrödinger-like equation of a two-level system,

$$i \frac{d}{dy} \begin{bmatrix} a_{1m} \\ a_{2n} \end{bmatrix} = \begin{bmatrix} 0 & C_{12} e^{iy\Delta} \\ C_{21} e^{-iy\Delta} & 0 \end{bmatrix} \begin{bmatrix} a_{1m} \\ a_{2n} \end{bmatrix},\quad (7)$$

where $\Delta = \beta_{1m} - \beta_{2n}$. It is important to note that equations (6) and (7) are the master coupling equation for determining the coupling between m th mode and n th mode in source/drain graphene electron waveguide studied in this paper. They are valid for the coupling of any dual-graphene electron waveguide device.

Before presenting the results, it is important to note that graphene is used as the electron waveguide channel and GaAs is the material for the potential barrier. The electrons inside the graphene waveguide channels are described by Dirac equation and Schrödinger equation is used to describe electrons dynamics in the potential barrier (GaAs). Previous work on single graphene electron waveguide channel [18, 19, 31, 33] has shown that the evanescent electron wave will exponentially decay outside of graphene electron waveguide. According to Hartmann's [19] and Xu's [34] papers, there are two kinds of stable modes in graphene electron waveguide dependent on two sub-lattice modes: ψ_A and ψ_B , where $\psi_A + i\psi_B$ is anti-symmetric and $\psi_A - i\psi_B$ is symmetric. The coupling between the same anti-symmetric functions, and the coupling between the antisymmetric and symmetric functions is, respectively, 0.24 meV and 0.14 meV, which are much smaller than the coupling between the two symmetric functions (1.58 meV).

Thus, we only consider the coupling of two symmetric functions in this paper. In figure 2, we show the symmetric wave function of the graphene electron waveguide at the different width of the waveguide: $d = 200, 300, 400,$ and 500 nm. The probability current density through the interface of graphene and GaAs is conserved [35]. Unless specified, the default parameters are $V_0 = 500$ meV, $V_1 = V_2 = 450$ meV, and $k_1 d = 4.96\pi$ $k_{1x} = k_1 \cos(\theta_m)$ is defined as the wave vector in the x direction.

The coupling strength between two parallel graphene electron waveguides is shown in figure 3, where we have assigned $k_1 d = 4.96\pi$ and study the dependence as a function of spacing (D) between the waveguides and width of the waveguide d . From figure 3, the coupling strength is decreasing with increasing spacing of D from about 0 to 120 nm. The coupling also increases with decreasing d from 500 to 250 nm. For smaller $d = 250$ nm or smaller, the mode profile becomes flat, and the overlapping calculated by $\int_{-\infty}^{+\infty} u_{1m}(x)u_{2n}(x)dx$ initially decreases until reaching a critical point, which is determined by the energy and incident angle as well as barrier height of injected electron. Finally we show a contour plot of the transition frequency f_T as a function of the spacing D and d in figure 4.

Compared with prior electron switching devices based on AlGaAs/GaAs materials, our proposed design based on graphene waveguides will have larger coupling energy (around 15 meV) and faster operating frequency (<1 ps in terms of time scale) as shown in figure 4. Most importantly, our proposed device is able to operate at room temperature due to the long mean free path of electrons in the graphene as compared to AlGaAs/GaAs material.

3. Discussions

Previous graphene FET have the low on–off ratio at room temperature [36]. In spite of many efforts to improve their designs [9, 10, 37, 38], the on–off ratio of the graphene FET is still below 10^6 even at a relatively high voltage of the order of 5 V [9, 10]. From the results obtained above in this paper, our proposed design can behave as a FET, in which electrons coupling between the two waveguides can be controlled by the gate voltage. Typical values of the on–off ratio is presented in figure 5, in which we use $D = 50$ nm and $d = 200$ nm and $k_1 d = 4.96\pi$. From the figure, we see that the on–off ratio can exceed 10^6 .

From solving equations (6) and (7) numerically, we present the first and second coupling modes of the graphene waveguide in figure 6 for $d = 200$ nm and $D = 50$ nm. For simplicity, the detuning parameter is set at $\Delta = 0$ and thus $\Omega = C_{12} = C_{21}$. The Schottky barrier height between the graphene and the GaAs is 0.5 eV [24]. In general, higher barrier height will allow for a lower coupling strength Ω , and leads to a longer coupling length. We also assume that the symmetrical wave mode $\psi_A - i\psi_B$ is the initially populated mode in the source graphene waveguide, which can be coherently excited by the high-quality contact between the metal electrode and graphene.

Figure 6 clearly shows a demonstration of Rabi oscillations of the electrons probability amplitudes between the two graphene waveguides, in analogy to the dynamics of a two-level quantum mechanical system. The population of the different modes of the graphene waveguides depends on the gate-controlled guiding of the electrons into the source waveguide. If the electron injected into the source graphene waveguide has a wave packet perfectly matched at a certain

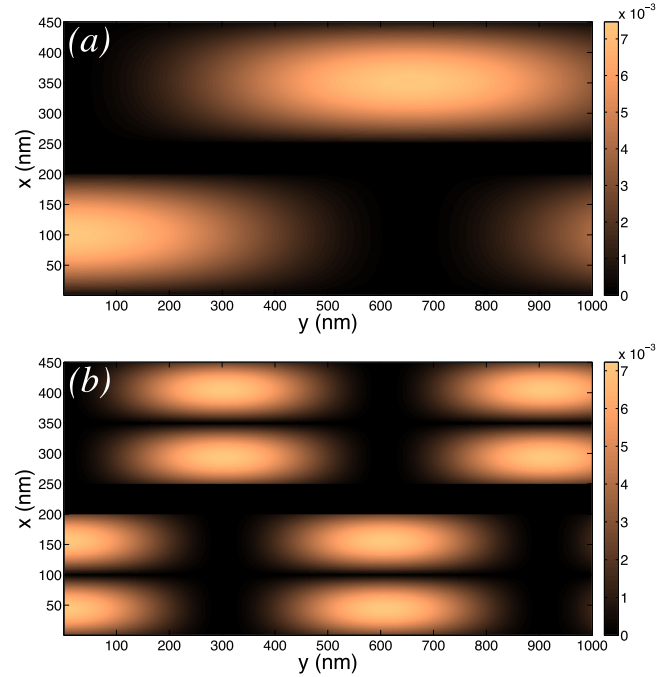


Figure 6. Electron wavefunction probability for a system of two coupled graphene electron waveguides. The parameters are set as follows: $d = 200$ nm, $D = 50$ nm, $k_1 d = 4.96\pi$ and the height of the barrier between graphene and GaAs (Si) is 500 meV and $V_1 = V_2 = 450$ meV. In the upper frame (a) we consider coupling between the first modes of the graphene waveguides, while in the lower frame (b) the coupling is between the corresponding second modes.

waveguide eigenstate, only that specific mode will be excited. The figure also demonstrates the electron coupling transfer length L up to 1000 nm is possible. As an example, the coupling between the first modes in quantum optical waveguides, the coupling length is $L = 654$ nm with a transfer frequency of $f_T = 1.53 \times 10^{12} \text{ s}^{-1}$ (or 0.65 ps), which is very fast (less than 1 ps).

These results show that the proposed electron switching device based on graphene electron waveguides has considerable advantages compared to similar devices using the conventional semiconductors materials in terms of operating speed, compactness and operating at room temperature. Note we do not consider higher-order coupling between the first mode in source waveguide and the second mode in the drain waveguide. The reasons are two folds: firstly, the coupling between the first mode (in the source waveguide) and second modes (in the drain waveguide) is asymmetric leading to very weak coupling strength (0.12 meV). Secondly, the preparation of modes in the waveguides (source or drain) depends on specified electron injection angles, so it is difficult to implement experimentally the coupling between these two modes. Interestingly, the coupling transfer length will be reduced to $L = 302$ nm and the transfer frequency will increase to $f_T = 3.3 \times 10^{12} \text{ s}^{-1}$ (0.3 ps) for coupling only between the second modes in the graphene electron waveguide, as shown in the figure 6(b).

CMT is a very powerful method to compute coupling strength, for which the only assumption is that two mode

profiles would not have changed during overlapping of two evanescent electric fields of two optical waveguides [28, 39]. The CMT not only works well for the electric field, also for electron wave function described by quantum mechanics. For example, the coupling mechanism of superconducting Josephson junctions can be described by CMT, as the evanescent wave function of electrons in two superconductors has overlapping [40]. Similarly, the CMT has also been utilized to describe the coupling between electronic waveguides based on AlGaAs/GaAs materials. Furthermore, the previous work on graphene electronic waveguide has already shown that wave function of electrons has the similar mode as the optical waveguide [17–21], (see electron wave function modes in graphene (figure 2)). Based on these arguments above, we believe that the CMT is valid for the description of the coupling mechanism between two parallel graphene electron waveguides.

There have been various papers [41–44] pointing out that Coulomb drag effect is very profound near the Dirac cone, which is induced by strong electron–electron interaction between two horizontal parallel graphene sheets separated by dielectric materials. However the graphene layout in our proposed device is coplanar parallel instead of horizontal parallel. Besides we focus on the condition that the Fermi level is far from the Dirac point. From the following simple analysis of Coulomb drag effect, we find that the Coulomb drag effect plays a minor role in our model.

When a current I_{active} flows on the active layer of graphene, it will induce a voltage V_{passive} on the passive layer of graphene, due to Coulomb drag effect, which can be measured by drag resistivity $\rho_{\text{drag}} = V_{\text{passive}}/I_{\text{active}}$. To numerically estimate the effect of the drag effect in our system, the drag resistivity ρ_{drag} based on Boltzmann transport formalism and the random phase approximation is used [43, 44], which is

$$\rho_{\text{drag}} = -\frac{1}{16\pi k_{\text{B}}T} \sum_q \int_0^\infty dw \frac{\Gamma_1(q, w)\Gamma_2(1, 2)|U_{1,2}(q, w)|^2}{\sinh^2(\hbar w/2k_{\text{B}}T)\sigma_{L_1}\sigma_{L_2}}. \quad (8)$$

Here, subscripts 1 and 2 are the labels for the two single-layer graphenes and Γ_i is the nonlinear susceptibility of layer i . $U_{1,2}$ is the screened interlayer potential in the random phase approximation. σ_{L_i} is the longitudinal conductivity of the layer i and k_{B} is the Boltzmann constant. The current flow I_2 in the passive graphene layer caused by Coulomb drag can be estimated as, $I_{\text{passive}} = \rho_{\text{drag}} I_1 \sigma d$, where $\sigma = \frac{4e^2 E_F \tau}{h} \frac{2}{\hbar}$ denotes the conductivity of the passive graphene layers [45], d is the width of our graphene layer and τ is the scattering time. For a typical set of parameters: $D = 50$ nm, $T = 300$ K, $d = 200$ nm and $E_F = 450$ meV, we get the ratio of $I_{\text{passive}}/I_{\text{active}}$ is 0.18%, which is extremely small. Thus the Coulomb drag effect in our model is negligible and will not greatly affect the calculations reported in this paper.

We have assumed that the phase-coherence of the electron waves is completely maintained in the course of tunneling, which is common practice in the study of mesoscopic physics. However, the electrons may suffer from scattering processes which cause momentum and energy relaxation

breaking the phase-coherence in the practical device structure. Usually, several possible causes exist for this sort of phase-coherence breaking scattering. One of them is residual impurity scattering. But our following estimation based on previous literature [46, 47] confirms that our assumption above is valid. The phase coherence length of electron can be estimated to be around 80 nm by using the most typical parameters for silicon and geometry setup of our device, which is larger than the 50 nm between two graphene electron waveguides used in our work. At the low temperature, the phase coherence length can be further improved (up to 18 μm) [48].

Conventional graphene electrical switches are mainly based on the FET [1–4], which utilizes the tunneling effect in the conduction channel between the source and drain electrodes. Unlike those conventional switches, the proposed electrical switch is not based on this traditional principle although its configuration is similar to conventional FET. The operating principle of our electrical switch depends on the electron wave coupling between the source graphene electron waveguide and the drain waveguide, which exhibits Rabi oscillations.

To check the sensitivity of the device against the fluctuations in the chemical potential, we assumed that the variation of the chemical potential is about 1 meV. Our calculations show that the resulting variation in the on–off ratio is less than 10%. Large chemical potential can ensure the stable operation of the proposed electrical switch without being affected by external environmental factors. The variation of 1 meV in the Fermi level may be justified by the large Fermi level. Previous paper [49] has reported that fluctuations in the carrier density induced by impurities in the environment or other factors disappear and chemical potential distribution becomes homogeneous when Fermi level is far from the neutral point in the graphene. If it is near the Dirac cone of the graphene, while fluctuations in the chemical potential may affect the operation of our device.

Additionally, the distance between two electron waveguide sets to be larger than 50 nm, so that the coupling between the two graphene sheets is too weak to open a gap in the graphene electronic bandstructure. Both theory and experiments have already confirmed that a very weak coupling between two separated graphene sheets cannot lead to a band gap if the gap distance between two graphene sheets is beyond 10 nm [50, 51]. Importantly, it is worth to emphasize that the proposed device operates at room temperature [45, 52], as a result, the exchange interaction between the electrons will be smeared out by large temperature fluctuations.

4. Conclusion

In summary, we have studied the coupling between two graphene electron waveguides by utilizing CMT. Based on this coupling mechanism, we have proposed an ultrafast electron switching device based on a dual-graphene-electron-waveguides structure. The performance of this design is

analyzed by using a modified couple model theory together with solving the Dirac and Schrödinger equations. Based on our model, it is possible to achieve higher operating frequency (less than 1 ps time scale) with short coupling transfer length at room temperature. This performance is better than the conventional design in using traditional AlGaAs/GaAs quantum well structure, which will also require very low operating temperature in order to have a long electron mean free path to ensure ballistic electron transport. The proposed design can be realized using current state-of-art-technology, for example single graphene electron waveguide channel has recently been fabricated with the gate-controlled guiding of electrons [21]. Our design resembles the traditional CMOS transistor in its layout, and thus its fabrication is feasible and it has the potential to contribute to the rapid development of quantum circuits and other integrated electron devices.

Acknowledgments

This work is partially supported by the Singapore ASTAR AME IRG (A1783c0011) and USA Air Force Office of Scientific Research (AFOSR) through the Asian Office of Aerospace Research and Development (AOARD) under Grant No. FA2386-17-1-4020. EK acknowledges financial support from the European Union's Horizon 2020 research and innovation programme under the Marie Skłodowska-Curie grant agreement No. 705256-COPQE.

Appendix

Firstly, we show that the Helmholtz-like equations (equation (3)) can be described as source/drain graphene electron waveguide in the y direction propagation. We take the source graphene electron waveguide as an example in our derivation and only consider single mode. Two sublattices A and B 's wavefunction of source graphene electron waveguide refer to as ψ_A and ψ_B . Electron is unbounded in the y -direction and electron's energy is $E \sin(\theta_1)$, where θ_1 is electron injection angle of source graphene electron waveguide. Based on the Dirac equations for free particles, we have

$$\begin{aligned} -i\hbar v_F \frac{\partial}{\partial y} \psi_B &= (E - V_1) \sin(\theta_1) \psi_A, \\ -i\hbar v_F \frac{\partial}{\partial y} \psi_A &= (E - V_1) \sin(\theta_1) \psi_B. \end{aligned} \quad (\text{A1})$$

Equation (A1) can be rewritten as $i\frac{\partial}{\partial y}\psi_B + \beta_1\psi_A = 0$ and $i\frac{\partial}{\partial y}\psi_A + \beta_1\psi_B = 0$, with $\beta_1 = (E - V_1)\sin(\theta_1)/\hbar v_F$. By taking the derivative on both side of the equations to decouple ψ_A and ψ_B , we obtain the Helmholtz-like equation for the source graphene electron waveguide: $\frac{\partial^2}{\partial y^2}\psi_A + \beta_1^2\psi_A = 0$ and $\frac{\partial^2}{\partial y^2}\psi_B + \beta_1^2\psi_B = 0$.

For source graphene electron waveguide, we only consider $\psi_1 = \psi_A - i\psi_B$, and the governing equation becomes

$\frac{\partial^2}{\partial y^2}\psi_1 + \beta_1^2\psi_1 = 0$. Repeat the same procedure, the Helmholtz-like equation for the drain graphene electron waveguide is obtained as $\frac{\partial^2}{\partial y^2}\psi_2 + \beta_2^2\psi_2 = 0$.

Below we show the derivation of equation (5) from (4) in the main text

$$\begin{aligned} \frac{\partial^2 \Psi_1}{\partial y^2} + \beta_1^2 \Psi_1 &= \frac{\partial^2 a_1}{\partial y^2} u_1(x) \exp(-i\beta_1 y) \\ &\quad - 2i\beta_1 \frac{\partial a_1}{\partial y} u_1(x) \exp(-i\beta_1 y) - \beta_1^2 a_1 u_1(x) \exp(-i\beta_1 y) \\ &\quad + \beta_1^2 a_1 u_1(x) \exp(-i\beta_1 y), \\ \frac{\partial^2 \Psi_2}{\partial y^2} + \beta_2^2 \Psi_2 &= \frac{\partial^2 a_2}{\partial y^2} u_2(x) \exp(-i\beta_2 y) \\ &\quad - 2i\beta_2 \frac{\partial a_2}{\partial y} u_2(x) \exp(-i\beta_2 y) - \beta_2^2 a_2 u_2(x) \exp(-i\beta_2 y) \\ &\quad + \beta_2^2 a_2 u_2(x) \exp(-i\beta_2 y). \end{aligned} \quad (\text{A2})$$

In equation (A2), we apply SEVA [32], say $\frac{d^2 a_1}{dy^2} \ll \frac{da_1}{dy}$ and $\frac{d^2 a_2}{dy^2} \ll \frac{da_2}{dy}$. The SEVA is a widely used method in the optics wave [28–30] and can also work for the electron wave function [55]. The SEVA is valid, when we assume that the envelope of a forward-traveling wave pulse varies slowly in time and space compared to a period or wavelength. The smallest envelope size in our device configuration can be estimated to be around 13 nm [53], much larger than wavelength of electron in graphene (about 0.74 nm) [54]. Therefore, the SEVA is a good approximation here. We can ignore the first term. The third term and fourth terms can be canceled out each other, based on equation (A2).

ORCID iDs

Shi-Jun Liang  <https://orcid.org/0000-0002-3466-8063>

References

- [1] Meric I, Han M Y, Young A F, Ozyilmaz B, Kim P and Shepard K L 2008 *Nat. Nanotechnol.* **3** 654–9
- [2] Avouris P 2010 *Nano Lett.* **10** 4285–94
- [3] Ni Z, Yu T, Lu Y, Wang Y, Feng Y and Shen Z 2008 *ACS Nano* **2** 2301–5
- [4] Zhou S Y, Gweon G, Fedorov A V, First P N, de Heer W A, Lee D H, Guinea F, Castro Neto A H and Lanzara A 2007 *Nat. Mater.* **6** 770–5
- [5] Zhang Y *et al* 2009 *Nature* **459** 820–3
- [6] Xia F, Farmer D, Lin Y and Avouris P 2010 *Nano Lett.* **10** 715–8
- [7] Chen S *et al* 2016 *Science* **353** 1522–5
- [8] Sajjad R and Avik W 2011 *Appl. Phys. Lett.* **99** 123101
- [9] Britnell L *et al* 2012 *Science* **335** 947–50
- [10] Ghobadi N and Pourfath M 2014 *IEEE Trans. Electron Devices* **61** 186–92
- [11] Alamo J A and Eugster C C 1990 *Appl. Phys. Lett.* **56** 78
- [12] Tsukada N, Wieck A D and Ploog K 1990 *Appl. Phys. Lett.* **56** 2527

- [13] Kroemer H and Okamoto H 1984 *Japan. J. Appl. Phys.* **23** 970
- [14] Alamo J A, Eugster C C, Hu Q, Melloch M R and Rooks M J 1998 *Superlattices Microstruct.* **23** 121
- [15] Eugster C C and Alamo J A 1991 *Phys. Rev. Lett.* **67** 3586
- [16] Liang W, Bockrath M, Bozovic D, Hafner J H, Tinkham M and Park H 2001 *Nature* **411** 665
- [17] Hrebikova I, Jelineka L, Vovesb J and Baenac J D 2014 *Phot. Nano. Fund. Appl.* **12** 9
- [18] Zhang F M, He Y and Chen X 2009 *Appl. Phys. Lett.* **94** 212105
- [19] Hartmann R R, Robinson N J and Portnoi M E 2010 *Phys. Rev. B* **81** 245431
- [20] Rickhaus P, Maurand R, Liu M, Weiss M, Richter K and Schonenberger C 2013 *Nat. Commun.* **4** 2342
- [21] Williams J R, Low T, Lundstrom M S and Marcus C M 2011 *Nat. Nanotechnol.* **6** 222
- [22] Allen M T, Shtanko O, Fulga I C, Akhmerov A R, Watanabe K, Taniguchi T, Jarillo-Herrero P, Levitov L S and Yacoby A 2016 *Nat. Phys.* **12** 128
- [23] Tongay S, Lemaitre M, Miao X, Gila B, Appleton B R and Hebard A F 2012 *Phys. Rev. X* **2** 011002
- [24] Bartolomeo A D 2016 *Phys. Rep.* **606** 1
- [25] Liang S J and Ang L K 2015 *Phys. Rev. Appl.* **3** 014002
- [26] Ang Y S and Ang L K 2016 *Phys. Rev. Appl.* **6** 034013
- [27] Morozov S V, Novoselov K S, Katsnelson M I, Schedin F, Elias D C, Jaszczak J A and Geim A K 2008 *Phys. Rev. Lett.* **100** 016602
- [28] Yariv A 1973 *IEEE J. Quantum Electron.* **9** 919
- [29] Longhi S 2005 *Phys. Rev. A* **71** 065801
- [30] Huang W, Rangelov A and Kyoseva E 2014 *Phys. Rev. A* **90** 053837
- [31] Myoung N, Ihm G and Lee S J 2011 *Phys. Rev. B* **83** 113407
- [32] Teich M C and Saleh B 1991 *Fundamentals of Photonics* 3rd edn (New York: Wiley-Interscience)
- [33] Yuan J, Cheng Z, Zeng Q, Zhang J and Zhang J 2011 *J. Appl. Phys.* **110** 103706
- [34] Xu Y and Ang L K 2015 *J. Opt.* **17** 035005
- [35] Dragoman D 2013 *J. Appl. Phys.* **113** 214312
- [36] Schwierz F 2010 *Nat. Nanotechnol.* **5** 487–96
- [37] Wang Y P and Cheng H P 2015 *Phys. Rev. B* **91** 245307
- [38] Katkov V L and Osipov V A 2014 *Appl. Phys. Lett.* **104** 053102
- [39] Haus H and Huang W 1991 *Proc. IEEE* **79** 1505–18
- [40] Raghavan S, Smerzi A, Fantoni S and Shenoy S R 1999 *Phys. Rev. A* **59** 620
- [41] Gorbachev R V, Geim A K, Katsnelson M I, Novoselov K S, Tudorovskiy T, Grigorieva I V, MacDonald A H, Watanabe K, Taniguchi T and Ponomarenko L A 2012 *Nat. Phys.* **8** 896–901
- [42] Schutt M, Ostrovsky P M, Titov M, Gornyi I V, Narozhny B N and Mirlin A D 2013 *Phys. Rev. Lett* **110** 026601
- [43] Tse W, Hu B Y and Sarma S 2007 *Phys. Rev. B* **76** 081401
- [44] Kim S, Jo I, Nah J, Yao Z, Banerjee S K and Tutuc E 2011 *Phys. Rev. B* **83** 161401
- [45] Adam S, Hwang E H, Galitski V M and Das Sarma S 2007 *Proc. Natl Acad. Sci.* **104** 18392
- [46] Altshuler B, Aronov A and Khmelnitsky D 1982 *J. Phys. C: Solid State Phys.* **15** 7367
- [47] Aleiner I L, Altshuler B L and Gershenson M E 1999 *Waves Random Media* **9** 201
- [48] Topinka M *et al* 2001 *Nature* **410** 183
- [49] Hajaj E M, Shtempluk O, Kochetkov V, Razin A and Yaish Y E 2013 *Phys. Rev. B* **88** 045128
- [50] Magda G Z, Jin X, Hagymási I, Vancsó P, Osváth Z, Nemes-Incze P, Hwang C, Biró L P and Tapasztó L 2014 *Nature* **514** 608
- [51] Zhao J, Dai X, Dai Y, Zhao B and Xie M 2012 *J. Appl. Phys.* **111** 043714
- [52] Li Q, Hwang E H and Das Sarma S 2011 *Phys. Rev. B* **84** 115442
- [53] Shafraniuk S 2015 *Graphene: Fundamentals, Devices, and Applications* (Boca Raton, FL: CRC Press)
- [54] Meyer J C *et al* 2008 *Appl. Phys. Lett.* **92** 123110
- [55] Burt M G 1999 *J. Phys.: Condens. Matter* **11** 53